Absence of Magnetic Proximity Effect at the Interface of Bi_2Se_3 and $(Bi,Sb)_2Te_3$ with EuS

A. I. Figueroa,[1,*] F. Bonell,[1] M. G. Cuxart,[1,2] M. Valvidares,[3] P. Gargiani,[3] G. van der Laan,[4] A. Mugarza,[1,5] and S. O. Valenzuela[1,5,†]

[1]Catalan Institute of Nanoscience and Nanotechnology (ICN2), CSIC and BIST, Campus UAB, Bellaterra, 08193 Barcelona, Spain
[2]Universitat Autònoma de Barcelona (UAB), Bellaterra 08193, Spain
[3]ALBA Synchrotron Light Source, Barcelona 08290, Spain
[4]Diamond Light Source, Harwell Science and Innovation Campus, Didcot OX11 0DE, United Kingdom
[5]Institució Catalana de Recerca i Estudis Avançats (ICREA), Barcelona 08010, Spain

(Received 21 October 2019; revised 2 September 2020; accepted 16 October 2020; published 24 November 2020)

We performed x-ray magnetic circular dichroism (XMCD) measurements on heterostructures comprising topological insulators (TIs) of the $(Bi,Sb)_2(Se,Te)_3$ family and the magnetic insulator EuS. XMCD measurements allow us to investigate element-selective magnetic proximity effects at the very TI/EuS interface. A systematic analysis reveals that there is neither significant induced magnetism within the TI nor an enhancement of the Eu magnetic moment at such interface. The induced magnetic moments in Bi, Sb, Te, and Se sites are lower than the estimated detection limit of the XMCD measurements of $\sim 10^{-3}\ \mu_B$/at.

DOI: 10.1103/PhysRevLett.125.226801

The observation of the quantum anomalous Hall effect (QAHE) in magnetically doped topological insulators (TIs) has raised significant interest for applications in metrology [1,2]. Test measurements demonstrating QAHE quantization accuracy at a record level of better than 1 part-per-million have recently been reported [3]. However, the magnetic impurities are incorporated randomly in the TI lattice and the resulting disorder presumably reduces the temperature and currents at which the QAHE fully develops. It also leads to the observation of superparamagnetic phases and multidomain magnetization switching, which coincide with the QAHE and are not well understood [4]. In this context, imprinting magnetism by proximity effects in thin film heterostructures appears as a promising alternative [5–8] that could ensure the preservation of the TI crystalline quality and its bulk insulating properties. Magnetic proximity effects in heterostructures comprising TIs and magnetic insulators (MIs) have been intensively investigated using optical methods, electronic transport measurements, polarized neutron reflectivity, and muon spin spectroscopy [6–16]. Studied heterostructures include Bi_2Se_3/EuS, $(Bi,Sb)_2Te_3$/EuS, $Y_3Fe_5O_{12}$/$(Bi_xSb_{1-x})_2Te_3$, $Tm_3Fe_5O_{12}$/$(Bi_xSb_{1-x})_2Te_3$, Fe_3O_4/Bi_2Te_3, $Cr_2Ge_2Te_6$/$(Bi,Sb)_2Te_3$, and $(Zn,Cr)Te$/$(Bi,Sb)_2Te_3$/$(Zn,Cr)Te$, with the QAHE only reported in the latter [14]. However, the most intriguing results have been arguably observed in Bi_2Se_3/EuS, where experiments using spin-polarized neutron reflectivity [7] suggest an enhanced magnetic signal within Bi_2Se_3. They also indicate the persistence of large interfacial ferromagnetism that extends 2 nm into the TI interface up to room temperature, even though isolated EuS orders ferromagnetically only below 17 K [7]. Such results are remarkable and would make Bi_2Se_3/EuS a leading candidate for the observation of topological magnetoelectric phenomena and QAHE at high temperatures.

However, while the number of articles reporting signatures of ferromagnetic behavior in TI/EuS interfaces keeps on growing, topological phenomena have yet to be observed. The QAHE has been systematically demonstrated in Cr- and V-doped $(Bi,Sb)_2Te_3$ [1,2] despite that the ferromagnetic state appears to be much weaker than in Bi_2Se_3/EuS. In addition, first-principles calculations of the electronic band structure and magnetic ordering of the Bi_2Se_3/EuS interface did not find an induced magnetic moment in the TI or even a significant enhancement of the local magnetic moment of Eu [17,18]. The discrepancy between experiments and theoretical analysis in combination with the absence of direct experimental proof of locally induced magnetism in the TI underscores the need for further experimental investigations.

Electronic and magnetic information regarding microscopic interactions can be obtained using x-ray absorption spectroscopy (XAS) and x-ray magnetic circular dichroism (XMCD). These techniques have been successfully implemented to study magnetically doped TIs [19–27] and—most importantly—are able to detect element-specific magnetic moments that are induced in the host TI lattice [25,27]. In this Letter, we report XAS and XMCD measurements on TI/EuS interfaces, with TIs of the $(Bi,Sb)_2(Se,Te)_3$ family. In contrast to previous investigations, our systematic study provides fundamental local and element-selective information of the magnetic

moments associated with Eu, Bi, Sb, Se, and Te atoms. In agreement with theoretical reports, we find no indication of proximity-induced magnetism in the TI. This suggests that the magnetic signatures in TI/MI heterostructures which have been reported do not originate from induced ferromagnetic order in the TI atoms at the TI/MI interface.

The TI/EuS heterostructures were grown on single-crystal $BaF_2(111)$ substrates by molecular beam epitaxy under ultrahigh vacuum (UHV) with a base pressure $\sim 1 \times 10^{-10}$ Torr. Bi_2Se_3, Bi_2Te_3, Sb_2Te_3, and $(Bi, Sb)_2Te_3$ thin films with a thickness of 10 nm were grown by coevaporation of elemental Bi, Sb, Se, and Te (6N purity), following the procedure in Ref. [28]. After growing the TI layer, the samples were transferred in UHV to a second chamber where a layer of 5-nm thick EuS was deposited at room temperature using an electron-beam evaporator, as in Ref. [7]. A protective 2-nm thick Al capping layer was subsequently deposited in the same chamber and allowed to oxidize in air. Additional Sb_2Te_3/EuS, $Sb_2Te_3/Bi_2Se_3/EuS$, and $Bi_2Se_3/EuS(x)$ with $x = 1$ and 5 nm samples were capped with a 20-nm thick Se layer grown *in situ*, which was desorbed in the UHV preparation chamber for XAS measurements by heating the sample to ~180 °C. The structural and crystal quality of the films was assessed using *in situ* reflection high energy electron diffraction and *ex situ* x-ray diffraction and x-ray photoelectron spectroscopy (XPS) revealing epitaxial growth and sharp interfaces [29]. The macroscopic magnetic properties were studied by SQUID magnetometry [29].

XAS was performed using a 6-T magnet on beam line BL-29 (BOREAS) at the ALBA synchrotron (Spain), which provides a UHV sample environment with a base temperature of ~3 K. Measurements were focused on the $M_{4,5}$ edges of Eu (1110–1170 eV), Te (570–590 eV), Bi (2560–2700 eV), and Sb (525–545 eV), and $L_{2,3}$ edges of Se (1420–1460 eV). The XMCD signal was obtained by subtracting XAS spectra with the photon helicity vector antiparallel and parallel to the applied magnetic field. Measurements used total-electron-yield (TEY) detection, where the drain current was taken from the sample to the ground. The magnetic field was applied along the x-ray beam for two different geometries: normal incidence (perpendicular to the sample plane) and grazing incidence (30° off the sample plane).

Figure 1 depicts XAS and XMCD spectra at the Eu $M_{4,5}$ edges for grazing incidence at 3 K under 2 T magnetic field. The M_5 edge peak maximum intensity is normalized to unity in order to compare the spectra from different samples. XMCD is expressed in percentage of the average XAS. The line shape and amplitude of the normalized XAS and XMCD signals for all TI/EuS samples [Figs. 1(a) and 1(d)] are nearly identical, which indicates the same electronic and magnetic state of the Eu atoms. The Eu $M_{4,5}$ edges correspond to $3d \rightarrow 4f$ electronic transitions. In order to identify the Eu electronic state, the results

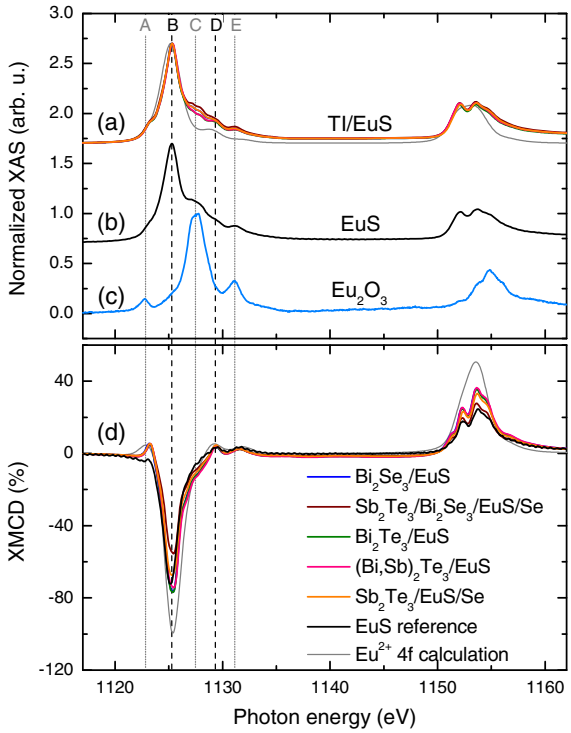

FIG. 1. (a) Averaged XAS spectra at the Eu $M_{4,5}$ edges for Bi_2Se_3/EuS, Bi_2Te_3/EuS, $(Bi, Sb)_2Te_3/EuS$, Sb_2Te_3/EuS, $Sb_2Te_3/EuS/Se$ samples and comparison with the spectrum calculated for Eu^{2+} $4f^7$, as well as (b) EuS and (c) Eu_2O_3 references. Reference spectra have been vertically shifted for clarity. (d) XMCD spectra for all samples and references. Dashed vertical lines mark the main features for Eu^{2+} (peaks *B* and *D*) and Eu^{3+} (peaks *A*, *C*, and *E*) around the M_5 edge. Measurements were performed at 3 K under 2 T magnetic field applied in grazing incidence.

are compared with the calculated spectra for Eu^{2+} $4f^7$ [Fig. 1(a) and Supplemental Material [29]] and the measured spectra in two reference samples: a 5-nm thick EuS thin film and Eu_2O_3 in powder form [Figs. 1(b) and 1(c), respectively]. The comparison reveals that spectra for all TI/EuS samples display the main features (peaks *B* and *D*) for Eu^{2+}, which is consistent with the expected electronic state for ferromagnetic EuS. Weak features corresponding to Eu^{3+} (peaks *A*, *C*, and *E*) are also visible, revealing some degree of Eu oxidation (Eu_2O_3 phase) at the surface of the sample, which is also observed and estimated to be between 0.35–0.47 nm thick by XPS [29]. Eu_2O_3 is not ferromagnetic, therefore it does not contribute to the XMCD signal [37].

XMCD is a powerful tool that yields the spin and orbital moments of the probed elements through the application of the magnetooptical sum rules [38,39]. For the rare earths, however, the sum rule analysis is less straightforward [40,41]. Since the XMCD intensity scales with the magnetization [41], values for the Eu $4f$ magnetic moments can be directly obtained by comparing the M_5 XMCD asymmetry with the expected theoretical value. This asymmetry

TABLE I. Effective magnetic moments for the Eu^{2+} $4f^7$ state in TI/EuS samples as derived from the Eu M_5 XMCD asymmetry. Measurements were recorded at 3 K, except for those marked with *, which were recorded at ~10 K. The local spin magnetic moment of Eu in Bi_2Se_3/EuS for the atomic ground state and as calculated by DFT [18] are included for comparison.

Sample	$\mu_{\mathrm{eff}}(\mu_B/\mathrm{atom})$
EuS	5.8 ± 0.3
Sb_2Te_3/EuS/Se	5.4 ± 0.3
Bi_2Te_3/EuS	6.1 ± 0.4
$(Bi, Sb)_2Te_3$/EuS	5.9 ± 0.3
Bi_2Se_3/EuS	6.1 ± 0.4
Sb_2Te_3/Bi_2Se_3/EuS/Se	4.4 ± 0.4
Bi_2Se_3/EuS (1 nm)/Se*	4.8 ± 0.4
Bi_2Se_3/EuS (5 nm)/Se*	5.3 ± 0.4
Atomic Hund's rule ground state	7.93
DFT calculation [18]	6.94

A is the maximum value of (XMCD)/(XAS sum), where XMCD and XAS are the difference and the sum, respectively, of the right- and left-circularly polarized XAS spectra at the Eu M_5 edge.

Table I lists the magnetic moments derived from A for each sample at 3 K (~10 K for Bi_2Se_3/EuS(x) with $x = 1$ and 5 nm samples). The calculated XMCD spectrum in Fig. 1(d) yields the theoretical asymmetry $A_{\mathrm{theory}} = -0.497$, which corresponds to the Hund's rule ground state (GS) value for Eu^{2+} $4f^7$ ($S = 7/2$, $L = 0$, $J = 7/2$), with an effective magnetic moment $\mu_{\mathrm{eff}}^{\mathrm{GS}} = 7.93$ μ_B. Because $L = 0$, this is a pure spin moment. Table I shows a reduction of μ_{eff} of about 30%–35% for all samples with respect to $\mu_{\mathrm{eff}}^{\mathrm{GS}}$, which could be due to the presence of a small crystal field acting on the Eu $4f$ electrons, as observed for other rare earths [42]. These values are well in agreement with the magnetic moments of Eu in Bi_2Se_3/EuS calculated by density functional theory [18], also included in Table I. No significant enhancement in the Eu $4f$ magnetic moments of our TI/EuS samples is found compared to that of the isolated EuS layer. This observation is consistent with theoretical reports [17,18], but contrary to experimental findings using polarized neutron reflectometry [7].

Magnetic hysteresis loops were recorded by fixing the energy at the maximum of the Eu M_5 XMCD signal (1125.4 eV) while sweeping the field. Figure 2 shows loops measured for Bi_2Te_3/EuS, Sb_2Te_3/EuS/Se, and Bi_2Se_3/EuS in grazing incidence. Values of A at saturation are very similar in all cases. This is consistent with Eu atoms having the same electronic and magnetic state regardless of the TI they are in contact with. The square shape of these hysteresis loops demonstrates that Eu $4f$ states are ferromagnetic at low temperatures (3 K) but they become paramagnetic at 20 K. This is in agreement with results of SQUID magnetometry, which indicate

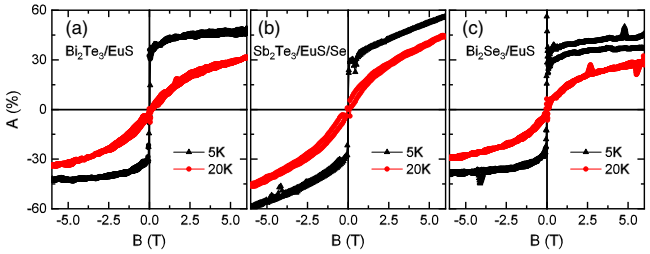

FIG. 2. Hysteresis loops recorded at the Eu M_5 edge for (a) Bi_2Te_3/EuS, (b) Sb_2Te_3/EuS/Se, and (c) Bi_2Se_3/EuS samples, measured in grazing incidence at 3 K (black triangles) and 20 K (red circles).

ferromagnetic ordering below $T_C \approx 15$ K [29]. Therefore, we do not observe signs of room-temperature ferromagnetic behavior in these TI/EuS systems, in contrast to previous reports [7].

The magnetic anisotropy of the Eu layer in the TI/EuS system was analyzed by comparing the XMCD spectra recorded in normal and grazing geometries at 2 T and at remanence (see Fig. S5 in Supplemental Material [29]). At 2 T, curves for normal and grazing geometries overlap for all TI/EuS samples. Without magnetic field, we observe remanence only in samples with the TI underlayer; the isolated EuS layer shows no XMCD signal at zero field. This behavior can be ascribed to the large spin-orbit interaction that is intrinsic to the TI [18]. Moreover, there is a significantly larger remanence in the grazing geometry for all TI/EuS samples, which is indicative of a favorable magnetization axis in the plane of the sample. In-plane anisotropy is also observed macroscopically by SQUID magnetometry (see Fig. S4 in Supplemental Material [29]). Previous experiments on Bi_2Se_3/EuS demonstrated perpendicular anisotropy in EuS [7]. Theoretical calculations have shown that topological surface states and their large intrinsic spin-orbit coupling may explain this observation [18]. However, the orientation of the magnetization depends strongly on the strain at the interface. When the EuS lattice is relaxed, as is the case for our TI/EuS films (see Fig. S1 in Supplemental Material [29]), it is expected that the magnetization remains in plane [18].

Next we will focus on the magnetic proximity effects. XMCD measurements at accessible absorption edges of Bi, Te, Sb, and Se elements were performed in search of induced magnetism on these nonmagnetic atoms. Figure 3 depicts XAS and XMCD spectra at the Bi $M_{4,5}$ and Se L_3 edges for Bi_2Se_3/EuS and at the Sb and Te M_5 edges for Sb_2Te_3/EuS. No XMCD signal is apparent in any of these absorption edges probed, remaining within the noise level.

TEY-detected XAS for soft x rays is a surface sensitive technique with the majority of electrons originating from within 3–5 nm [41,43]. This implies that the XAS signal not only arises from the uppermost region of the TI, which is in contact with EuS, but also from the bulk of the film with a contribution that decreases exponentially with depth.

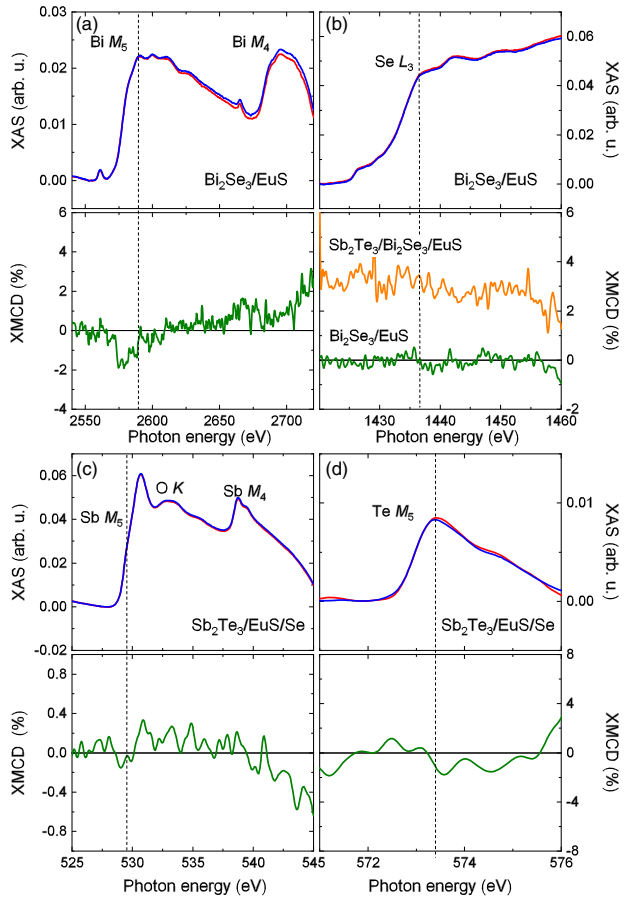

FIG. 3. Experimental spectra for left- and right-circularly polarized x rays. XAS (top panel) and XMCD (bottom panel) at the (a) Bi $M_{4,5}$ and (b) Se L_3 edges for Bi_2Se_3/EuS and the (c) Sb $M_{4,5}$ and (d) Te M_5 edges for Sb_2Te_3/EuS. The XMCD signal at the Se L_3 edge for the Sb_2Te_3/Bi_2Se_3/EuS sample has been included in (b) for comparison (vertically shifted for clarity). Measurements were performed at 3 K under a magnetic field of 2 T applied along the normal. Dashed lines mark the energy at which the XMCD features are expected to appear.

In order to verify the absence of proximity-induced magnetism, we performed XMCD measurements at the Se L_3 and Bi $M_{4,5}$ edges in a Sb_2Te_3/Bi_2Se_3/EuS heterostructure. The Bi_2Se_3 layer is 1 nm thick, ensuring that the recorded XAS signal originates from the very Bi_2Se_3/EuS interface. XMCD at the Se L_3 edge for this sample is plotted in Fig. 3(b) (the Bi signal on this sample, not shown, is very weak). In agreement with the results on the Bi_2Se_3/EuS, no XMCD signal is found at this absorption edge.

Non-negligible Te and Sb XMCD signals have been reported for thin films of Cr-doped Sb_2Te_3 [26,44] and bulk Cr-, V-, and Mn-doped Sb_2Te_3 [26,44] and Cr-doped $(Bi, Sb)_2Te_3$ [25,45]. In all these cases, XMCD data were recorded in TEY for *in situ* cleaved samples. TEY detected XAS and XMCD signals for our TI/EuS heterostructures have poor statistics compared to those reported for *in situ* cleaved samples due to the 5 nm EuS and 2 nm Al on top of the TI. Despite the noise level of the data, application of the magnetooptical sum rules [38,39] to the XAS and XMCD signal in Fig. 3 can provide an upper limit for the induced magnetic moment on Bi, Sb, Se, and Te atoms in contact with EuS [29]. We found values of the spin moment, $S_z \approx 10^{-3}$ μ_B per Bi and Se atom in the Bi_2Se_3/EuS samples and $\sim 10^{-3}$ μ_B per Sb and $\sim 10^{-4}$ μ_B per Te in the Sb_2Te_3/EuS/Se sample.

The negligible induced magnetic moment on Bi, Sb, Te, and Se atoms of $(Bi, Sb)_2(Se, Te)_3$ in contact with EuS is a surprising finding. Recent observations suggest the presence of magnetism within the TI layer of Bi_2Se_3/EuS by magnetotransport measurements [9,46], polarized neutron reflectometry [7,11], magnetic second-harmonic generation [10], and low-energy muon spin rotation [12]. Katmis *et al.* [7] reported values of magnetization in the TI for a Bi_2Se_3(20 QL)/EuS(5 nm) sample (QL stands for quintuple layer and is $\sim$1 nm thick) between 250 and 300 emu/cm^3, which correspond to a magnetic moment between 4.4 and 5.3 μ_B per QL in a unit cell of Bi_2Se_3. Assuming that Bi and Se atoms become equally magnetic, and that magnetism develops over a unit cell closest to EuS, the magnetic moment amounts to $\sim$0.88–1.06 μ_B per (Bi or Se) atom, which is about 2 to 3 orders of magnitude larger than those estimated for our Bi_2Se_3/EuS samples from XMCD measurements.

XMCD measurements have already been used to rule out reported proximity effects using other (nonelement selective) experimental techniques. For example, the anisotropic magnetoresistance at $Y_3Fe_5O_{12}$/Pt and ferrite/Pt interfaces was attributed to Pt atoms polarized by proximity effects. However, XMCD measurements at the Pt edges have shown no evidence of induced magnetism [47–49]. Theoretical studies using first-principles calculations show insignificant or no magnetism in the TI for Bi_2Se_3/EuS with ideally sharp interfaces [17,18,50], which is consistent with our XMCD results. Instead, Eu doping on Bi_2Se_3 could result in local magnetic moments that are much larger than those induced by the adjacent magnetic layer, possibly explaining the experimental observations [17]. One Eu atom diffusing into the TI per unit cell would account for an observed magnetic moment of $\sim$1 μ_B/at in a QL [17]. Intercalation of a single EuS layer has been theoretically predicted to be energetically favorable and leads to the observation of magnetism within the TI and, perhaps, of proximity effects, by suppressing the formation of trivial states [51]. However, our data does not show evidence of such an intercalation. Other interfacial effects, including charge transfer at the TI/MI interface and band bending could explain the absence of induced magnetism in the TI and the lack of observation of the QAHE [51–55]. Another possibility for the absence of proximity effects would be the presence of a magnetic dead layer at the TI/EuS interface. However, XAS and XMCD measurements of ultrathin EuS

layers (≤ 1 nm) grown onto Bi_2Se_3 reveal that EuS remains magnetic, which allowed us to exclude such scenario in our TI/EuS samples [29]. This conclusion is further supported by the increase of the in-plane magnetic remanence for the TI/EuS structures, compared to the isolated EuS layer, which can be ascribed to the large intrinsic spin-orbit interaction of the TI at a sharp TI/EuS interface [18].

In summary, we have performed element-selective magnetometry to study proximity effects at the interface of TI/EuS bilayers. A variety of TIs of the $(Bi, Sb)_2(Se, Te)_3$ family were systematically investigated. The easy-magnetization axis of EuS remains in the plane of the sample and the magnetic remanence increases as a result of its contact with the TI. However, we found no evidence for an enhancement of Eu magnetic moments in the EuS layer, or an increase in the ferromagnetic ordering temperature. The magnetic signals on Bi, Sb, Te, and Se atoms of the TIs in contact with EuS were found to be negligible (below the detection limit of the XMCD technique) at temperatures and conditions where the EuS is magnetic and could polarize these nonmagnetic atoms. Overall our XMCD measurements suggest that the observations in TI/EuS interfaces by magnetotransport and optical techniques are not due to proximity-induced magnetism but to a different mechanism, such as magnetic doping by Eu diffusion into the TI.

This research was supported by the European Union's Horizon 2020 FET-PROACTIVE project TOCHA under Grant Agreement 824140. The authors acknowledge funding by the European Research Council under Grant Agreement No. 306652 SPINBOUND, by the CERCA Programme/Generalitat de Catalunya 2017 SGR 827, by MINECO (under Contracts No. MAT2016-75952-R, No. MAT2016-78293-C6-2-R, No. PID2019-111773RB-I00/AEI/10.13039/501100011033, No. PID2019-107338RB-C65, and Severo Ochoa No. SEV-2017-0706) and the European Regional Development Fund (ERDF) under the program Interreg V-A España-Francia-Andorra (Contract No. EFA 194/16 TNSI). A. I. F. acknowledges funding from MINECO-Juan de la Cierva fellowship ref. IJCI-2015-25514 and from the European Union's Horizon 2020 People Programme (Marie Skłodowska Curie Actions) H2020-MSCA-IF-2017 under REA Grant Agreement No. 796925. F. B. acknowledges funding from MINECO Ramón y Cajal Program under Contract No. RYC-2015-18523. We acknowledge beam time on BOREAS (BL29) beam line at ALBA Synchrotron under proposal 2017022019.

*adriana.figueroa@icn2.cat
†SOV@icrea.cat

[1] C. Z. Chang *et al.*, Experimental observation of the quantum anomalous Hall effect in a magnetic topological insulator, Science **340**, 167 (2013).
[2] C. Z. Chang, W. Zhao, D. Y. Kim, H. Zhang, B. A. Assaf, D. Heiman, S. C. Zhang, C. Liu, M. H. W. Chan, and J. S. Moodera, High-precision realization of robust quantum anomalous Hall state in a hard ferromagnetic topological insulator, Nat. Mater. **14**, 473 (2015).
[3] M. Götz, K. M. Fijalkowski, E. Pesel, M. Hartl, S. Schreyeck, M. Winnerlein, S. Grauer, H. Scherer, K. Brunner, C. Gould, F. J. Ahlers, and L. W. Molenkamp, Precision measurement of the quantized anomalous Hall resistance at zero magnetic field, Appl. Phys. Lett. **112**, 072102 (2018).
[4] M. Winnerlein, S. Schreyeck, S. Grauer, S. Rosenberger, K. M. Fijalkowski, C. Gould, K. Brunner, and L. W. Molenkamp, Epitaxy and structural properties of $(V, Bi, Sb)_2Te_3$ layers exhibiting the quantum anomalous Hall effect, Phys. Rev. Mater. **1**, 011201(R) (2017).
[5] M. Li, C. Z. Chang, B. J. Kirby, M. E. Jamer, W. Cui, L. Wu, P. Wei, Y. Zhu, D. Heiman, J. Li, and J. S. Moodera, Proximity-Driven Enhanced Magnetic Order at Ferromagnetic-Insulator—Magnetic-Topological-Insulator Interface, Phys. Rev. Lett. **115**, 087201 (2015).
[6] Z. Jiang, C.-Z. Chang, C. Tang, P. Wei, J. S. Moodera, and J. Shi, Independent tuning of electronic properties and induced ferromagnetism in topological insulators with heterostructure approach, Nano Lett. **15**, 5835 (2015).
[7] F. Katmis, V. Lauter, F. S. Nogueira, B. A. Assaf, M. E. Jamer, P. Wei, B. Satpati, J. W. Freeland, I. Eremin, D. Heiman, P. Jarillo-Herrero, and J. S. Moodera, A high-temperature ferromagnetic topological insulating phase by proximity coupling, Nature (London) **533**, 513 (2016).
[8] C. Tang, C.-Z. Chang, G. Zhao, Y. Liu, Z. Jiang, C.-X. Liu, M. R. McCartney, D. J. Smith, T. Chen, J. S. Moodera, and J. Shi, Above 400-K robust perpendicular ferromagnetic phase in a topological insulator, Sci. Adv. **3**, e1700307 (2017).
[9] P. Wei, F. Katmis, B. A. Assaf, H. Steinberg, P. Jarillo-Herrero, D. Heiman, and J. S. Moodera, Exchange-coupling-induced symmetry breaking in topological insulators, Phys. Rev. Lett. **110**, 186807 (2013).
[10] C. Lee, F. Katmis, P. Jarillo-Herrero, J. S. Moodera, and N. Gedik, Direct measurement of proximity-induced magnetism at the interface between a topological insulator and a ferromagnet, Nat. Commun. **7**, 12014 (2016).
[11] M. Li, Q. Song, W. Zhao, J. A. Garlow, T.-H. Liu, L. Wu, Y. Zhu, J. S. Moodera, M. H. W. Chan, G. Chen, and C.-Z. Chang, Dirac-electron-mediated magnetic proximity effect in topological insulator/magnetic insulator heterostructures, Phys. Rev. B **96**, 201301(R) (2017).
[12] J. A. Krieger, Y. Ou, M. Caputo, A. Chikina, M. Döbeli, M.-A. Husanu, I. Keren, T. Prokscha, A. Suter, C.-Z. Chang, J. S. Moodera, V. N. Strocov, and Z. Salman, Do topology and ferromagnetism cooperate at the EuS/Bi_2Se_3 interface? Phys. Rev. B **99**, 064423 (2019).
[13] M. Mogi, T. Nakajima, V. Ukleev, A. Tsukazaki, R. Yoshimi, M. Kawamura, K. S. Takahashi, T. Hanashima, K. Kakurai, T.-h. Arima, M. Kawasaki, and Y. Tokura, Large Anomalous Hall Effect in Topological Insulators with Proximitized Ferromagnetic Insulators, Phys. Rev. Lett. **123**, 016804 (2019).
[14] R. Watanabe, R. Yoshimi, M. Kawamura, M. Mogi, A. Tsukazaki, X. Z. Yu, K. Nakajima, K. S. Takahashi, M.

Kawasaki, and Y. Tokura, Quantum anomalous hall effect driven by magnetic proximity coupling in all-telluride based heterostructure, Appl. Phys. Lett. **115**, 102403 (2019).
[15] S. Mathimalar, S. Sasmal, P. Rajasekhar, A. Bhardwaj, S. Chaudhary, B. Satpati, and K. V. Raman, Evidence of topological gap opening in the surface state of Bi_2Se_3 by proximity to a magnetic insulator, arXiv:1907.12770.
[16] V. M. Pereira, S. G. Altendorf, C. E. Liu, S. C. Liao, A. C. Komarek, M. Guo, H.-J. Lin, C. T. Chen, M. Hong, J. Kwo, L. H. Tjeng, and C. N. Wu, Topological insulator interfaced with ferromagnetic insulators: Bi_2Te_3 thin films on magnetite and iron garnets, Phys. Rev. Mater. **4**, 064202 (2020).
[17] S. V. Eremeev, V. N. Men'shov, V. V. Tugushev, and E. V. Chulkov, Interface induced states at the boundary between a 3D topological insulator Bi_2Se_3 and a ferromagnetic insulator EuS, J. Magn. Magn. Mater. **383**, 30 (2015).
[18] J. Kim, K.-W. Kim, H. Wang, J. Sinova, and R. Wu, Understanding the Giant Enhancement of Exchange Interaction in Bi_2Se_3-EuS Heterostructures, Phys. Rev. Lett. **119**, 027201 (2017).
[19] A. I. Figueroa, G. van der Laan, L. J. Collins-McIntyre, S.-L. Zhang, A. A. Baker, S. E. Harrison, P. Schönherr, G. Cibin, and T. Hesjedal, Magnetic Cr doping of Bi_2Se_3: Evidence for divalent Cr from x-ray spectroscopy, Phys. Rev. B **90**, 134402 (2014).
[20] W. Liu, D. West, L. He, Y. Xu, J. Liu, K. Wang, Y. Wang, G. van der Laan, R. Zhang, S. Zhang, and K. L. Wang, Atomic-scale magnetism of Cr-doped Bi_2Se_3 thin film topological insulators, ACS Nano **9**, 10237 (2015).
[21] S. E. Harrison, L. J. Collins-McIntyre, S. L. Zhang, A. A. Baker, A. I. Figueroa, A. J. Kellock, S. S. P. Parkin, J. S. Harris, G. van der Laan, and T. Hesjedal, Study of Dy-doped Bi_2Te_3: Thin film growth and magnetic properties, J. Phys. Condens. Matter **27**, 245602 (2015).
[22] S. E. Harrison, L. J. Collins-McIntyre, S. L. Zhang, A. A. Baker, A. I. Figueroa, A. J. Kellock, A. Pushp, Y. L. Chen, S. S. P. Parkin, J. S. Harris, G. van der Laan, and T. Hesjedal, Study of Ho-doped Bi_2Te_3 topological insulator thin films, Appl. Phys. Lett. **107**, 182406 (2015).
[23] W. Q. Liu, L. He, Y. B. Xu, K. Murata, M. C. Onbasli, M. Lang, N. J. Maltby, S. Li, X. Wang, C. A. Ross, P. Bencok, G. van der Laan, R. Zhang, and K. L. Wang, Enhancing magnetic ordering in Cr-doped Bi_2Se_3 using high-T_C ferrimagnetic insulator, Nano Lett. **15**, 764 (2015).
[24] A. A. Baker, A. I. Figueroa, K. Kummer, L. J. Collins-McIntyre, T. Hesjedal, and G. van der Laan, Magnetic proximity-enhanced Curie temperature of Cr-doped Bi_2Se_3 thin films, Phys. Rev. B **92**, 094420 (2015).
[25] M. Ye, W. Li, S. Zhu, Y. Takeda, Y. Saitoh, J. Wang, H. Pan, M. Nurmamat, K. Sumida, F. Ji, Z. Liu, H. Yang, Z. Liu, D. Shen, A. Kimura, S. Qiao, and X. Xie, Carrier-mediated ferromagnetism in the magnetic topological insulator Cr-doped $(Sb, Bi)_2Te_3$, Nat. Commun. **6**, 8913 (2015).
[26] L. B. Duffy, A. I. Figueroa, L. Gladczuk, N.-J. Steinke, K. Kummer, G. van der Laan, and T. Hesjedal, Magnetic proximity coupling to Cr-doped Sb_2Te_3 thin films, Phys. Rev. B **95**, 224422 (2017).
[27] P. Rüßmann, S. K. Mahatha, P. Sessi, M. A. Valbuena, T. Bathon, K. Fauth, S. Godey, A. Mugarza, K. A. Kokh, O. E. Tereshchenko, P. Gargiani, M. Valvidares, E. Jiménez, N. B. Brookes, M. Bode, G. Bihlmayer, S. Blgel, P. Mavropoulos, C. Carbone, and A. Barla, Towards microscopic control of the magnetic exchange coupling at the surface of a topological insulator, J. Phys. Mater. **1**, 015002 (2018).
[28] F. Bonell, M. G. Cuxart, K. Song, R. Robles, P. Ordejón, S. Roche, A. Mugarza, and S. O. Valenzuela, Growth of twin-free and low-doped topological insulators on $BaF_2(111)$, Cryst. Growth Des. **17**, 4655 (2017).
[29] See Supplemental Material at http://link.aps.org/supplemental/10.1103/PhysRevLett.125.226801 for structural and magnetic characterization of the $(Bi, Sb)_2(Se, Te)_2$/EuS samples using in situ RHEED, *ex situ* XRD, XPS, and SQUID magnetometry, which includes Refs. [30–36].
[30] R. Vercaemst, D. Poelman, L. Fiermans, R. L. Van Meirhaeghe, W. H. Laflre, and F. Cardon, A detailed XPS study of the rare earth compounds EuS and EuF_3, J. Electron Spectrosc. Relat. Phenom. **74**, 45 (1995).
[31] B. R. Strohmeier, An ESCA method for determining the oxide thickness on aluminum alloys, Surf. Interface Anal. **15**, 51 (1990).
[32] T. A. Carlson and G. E. McGuire, Study of the x-ray photoelectron spectrum of tungsten-tungsten oxide as a function of thickness of the surface oxide layer, J. Electron Spectrosc. Relat. Phenom. **1**, 161 (1972).
[33] P. Ngabonziza, R. Heimbuch, N. de Jong, R. A. Klaassen, M. P. Stehno, M. Snelder, A. Solmaz, S. V. Ramankutty, E. Frantzeskakis, E. van Heumen, G. Koster, M. S. Golden, H. J. W. Zandvliet, and A. Brinkman, In situ spectroscopy of intrinsic Bi_2Te_3 topological insulator thin films and impact of extrinsic defects, Phys. Rev. B **92**, 035405 (2015).
[34] B. T. Thole, G. van der Laan, J. C. Fuggle, G. A. Sawatzky, R. C. Karnatak, and J. M. Esteva, $3d$ x-ray absorption lines and the $3d^9 4f^{n+1}$ multiplets of the lantanides, Phys. Rev. B **32**, 5107 (1985).
[35] G. van der Laan, Hitchhiker's guide to multiplet calculations, Lect. Notes Phys. **697**, 143 (2006).
[36] R. D. Cowan, *The Theory of Atomic Structure and Spectra* (University of California Press, Berkeley, 1981).
[37] E. Negusse, J. Dvorak, J. S. Holroyd, M. Liberati, T. S. Santos, J. S. Moodera, E. Arenholz, and Y. U. Idzerda, Magnetic characterization of ultrathin EuO films with xmcd, J. Appl. Phys. **105**, 07C930 (2009).
[38] B. T. Thole, P. Carra, F. Sette, and G. van der Laan, X-Ray Circular Dichroism as a Probe of Orbital Magnetization, Phys. Rev. Lett. **68**, 1943 (1992).
[39] P. Carra, B. T. Thole, M. Altarelli, and X. Wang, X-Ray Circular Dichroism and Local Magnetic Fields, Phys. Rev. Lett. **70**, 694 (1993).
[40] G. van der Laan, Sum rule practice, J. Synchrotron Radiat. **6**, 694 (1999).
[41] G. van der Laan and A. I. Figueroa, X-ray magnetic circular dichroism—A versatile tool to study magnetism, Coord. Chem. Rev. **277–278**, 95 (2014).
[42] A. I. Figueroa, A. A. Baker, S. E. Harrison, K. Kummer, G. van der Laan, and T. Hesjedal, X-ray magnetic circular dichroism study of Dy-doped Bi_2Te_3 topological insulator thin films, J. Magn. Magn. Mater. **422**, 93 (2017).
[43] J. Stöhr and H. C. Siegmann, *Magnetism. From Fundamentals to Nanoscale Dynamics* (Springer-Verlag, Berlin, Heidelberg, 2006), https://doi.org/10.1007/978-3-540-30283-4.

[44] M. F. Islam *et al.*, Systematics of electronic and magnetic properties in the transition metal doped Sb_2Te_3 quantum anomalous Hall platform, Phys. Rev. B **97**, 155429 (2018).

[45] M. Ye, T. Xu, G. Li, S. Qiao, Y. Takeda, Y. Saitoh, S.-Y. Zhu, M. Nurmamat, K. Sumida, Y. Ishida, S. Shin, and A. Kimura, Negative Te spin polarization responsible for ferromagnetic order in the doped topological insulator $V_{0.04}(Sb_{1-x}Bi_x)_{1.96}Te_3$, Phys. Rev. B **99**, 144413 (2019).

[46] Q. I. Yang and A. Kapitulnik, Two-stage proximity-induced gap opening in topological-insulator–insulating-ferromagnet $(Bi_xSb_{1-x})_2Te_3$–EuS bilayers, Phys. Rev. B **98**, 081403 (R) (2018).

[47] S. Geprägs, S. Meyer, S. Altmannshofer, M. Opel, F. Wilhelm, A. Rogalev, R. Gross, and S. T. B. Goennenwein, Investigation of induced Pt magnetic polarization in $Pt/Y_3Fe_5O_{12}$ bilayers, Appl. Phys. Lett. **101**, 262407 (2012).

[48] M. Valvidares, N. Dix, M. Isasa, K. Ollefs, F. Wilhelm, A. Rogalev, F. Sánchez, E. Pellegrin, A. Bedoya-Pinto, P. Gargiani, L. E. Hueso, F. Casanova, and J. Fontcuberta, Absence of magnetic proximity effects in magnetoresistive $Pt/CoFe_2O_4$ hybrid interfaces, Phys. Rev. B **93**, 214415 (2016).

[49] M. Collet, R. Mattana, J.-B. Moussy, K. Ollefs, S. Collin, C. Deranlot, A. Anane, V. Cros, F. Petroff, F. Wilhelm, and A. Rogalev, Investigating magnetic proximity effects at ferrite/Pt interfaces, Appl. Phys. Lett. **111**, 202401 (2017).

[50] H. L. Meyerheim, A. Ernst, K. Mohseni, A. Polyakov, I. V. Maznichenko, P. A. Buczek, A. Coati, and S. S. P. Parkin, Structure and magnetism of EuS on $Bi_2Se_3(0001)$, Phys. Status Solidi B 2000290 (2020).

[51] S. V. Eremeev, M. M. Otrokov, and E. V. Chulkov, New universal type of interface in the magnetic insulator/topological insulator heterostructures, Nano Lett. **18**, 6521 (2018).

[52] V. N. Men'shov, V. V. Tugushev, S. V. Eremeev, P. M. Echenique, and E. V. Chulkov, Magnetic proximity effect in the three-dimensional topological insulator/ferromagnetic insulator heterostructure, Phys. Rev. B **88**, 224401 (2013).

[53] S. V. Eremeev, V. N. Men'shov, V. V. Tugushev, P. M. Echenique, and E. V. Chulkov, Magnetic proximity effect at the three-dimensional topological insulator/magnetic insulator interface, Phys. Rev. B **88**, 144430 (2013).

[54] V. N. Men'shov, I. A. Shvets, and E. V. Chulkov, Interface effects on the magnetic-proximity-induced quantized hall response in heterostructures based on three-dimensional topological insulators, Phys. Rev. B **99**, 115301 (2019).

[55] E. K. Petrov, I. V. Silkin, T. V. Menshchikova, and E. V. Chulkov, Cr-containing ferromagnetic film topological insulator heterostructures as promising materials for the quantum anomalous hall effect, JETP Lett. **109**, 121 (2019).